Protection of Coastal Shelter Forests Using UAVs: Individual Tree and Tree-Height Detection in *Casuarina equisetifolia* L. Forests

Lili Lin [1,2], **Zhenbang Hao** [3,*], **Christopher J. Post** [4] **and Elena A. Mikhailova** [4]

1 Department of Biological Science and Biotechnology, Minnan Normal University, Zhangzhou 363000, China
2 University Key Lab for Fujian and Taiwan Garden Plants in Fujian Province, Zhangzhou 363000, China
3 University Key Lab for Geomatics Technology and Optimized Resources Utilization in Fujian Province, Fuzhou 350002, China
4 Department of Forestry and Environmental Conservation, Clemson University, Clemson, SC 29634, USA
* Correspondence: zhenbanghao@fafu.edu.cn; Tel.: +86-059186392212

Abstract: *Casuarina equisetifolia* L. plays a significant role in sandy, coastal regions for sand stabilization and windbreaks. However, *C. equisetifolia* forests are susceptible to plant diseases and insect pests, resulting in mortality due to pure stands and a harsh natural environment. Mapping the distribution of *C. equisetifolia* and detecting its height can inform forest-management decisions. Unmanned aerial vehicle (UAV) imagery, coupled with the classical detection method, can provide accurate information on tree-level forest parameters. Considering that the accuracy of a forest-parameter estimation is impacted by various flight altitudes and extraction parameters, the purpose of this study is to determine the appropriate flight altitude and extraction parameters for mapping *C. equisetifolia* using UAV imagery and the local maxima algorithm in order to monitor *C. equisetifolia* more accurately. A total of 11 different flight altitudes and 36 combinations of circular smoothing window size (CSWS) and fixed circular window size (FCWS) were tested, and 796 trees with corresponding positions in the UAV image and ground–tree heights were used as reference. The results show that the combination of a 0.1 m CSWS and a 0.8 m FCWS for individual tree detection (ITD) and tree-height detection achieved excellent accuracy (with an *F*1 score of 91.44% for ITD and an estimation accuracy (*EA*) of 79.49% for tree-height detection). A lower flight altitude did not indicate a higher accuracy for individual tree and tree-height detection. The UAV image obtained within a flight altitude of 60 m–80 m can meet the accuracy requirements for the identification of *C. equisetifolia* tree-height estimation (*F*1 score > 85% for ITD; *EA* > 75% for tree-height estimation). This study provides a foundation for monitoring *C. equisetifolia* by using UAV imagery and applying the local maxima algorithm, which may help forestry practitioners detect *C. equisetifolia* trees and tree heights more accurately, providing more information on *C. equisetifolia* growth status.

Keywords: *Casuarina equisetifolia* L.; flight altitude; extraction parameters; coastal forest; local maxima method

1. Introduction

Casuarina equisetifolia L. is vital as a windbreak in coastal areas, with a wide natural range in Australia, Southeast Asia, and the Pacific Islands [1]. This tree species also has characteristics that include symbiotic nitrogen fixation [2,3], the ability to stabilize sandy soils [4,5], drought and salt resistance [6,7], soil quality improvement, and soil rehabilitation [2,8]. Thus, *C. equisetifolia* has become one of the most popular trees for blocking wind in sandy, coastal regions all over the world due to these various benefits [9,10]. In coastal shelter forests particularly, *C. equisetifolia* has the ability to protect farmland and houses from natural disasters such as wind erosion and tsunamis [11,12], and can prevent damage from drifting sand [10]. However, in some areas with a poor growing environment, *C. equisetifolia* trees are particularly susceptible to various disturbances and prone to growing difficulties. In this context, it is necessary to obtain accurate information on

C. equisetifolia forest stands for forest management [13]. Additionally, there is still a gap in the knowledge of how to optimize UAV flight and analysis parameters to measure tree characteristics for *C. equisetifolia*.

Individual trees and tree height are significant metrics for *C. equisetifolia* forest management, especially considering the height [14], density, open gaps [15,16], and structure [10,16], which can impact the sand stabilization and windbreak ability. A previous study reported that coastal vegetation was able to reduce the severity of a tsunami [10], however, open gaps reduced this feature of *C. equisetifolia* forests. Tree height determines the horizontal sheltered area, which is significant for reducing wind speed [17]. Zhang et al. [18] reported that quicksand can easily penetrate the forest belt and can cause sand damage if open gaps are formed inside the forest belt. Heisler and Dewalle found that, because the windbreak height reduces wind speed, the horizontal, sheltered area was determined by the windbreak height [17]. In addition, in the up-wind direction of the windward side of a forest, the shelter area could extend to a distance of five times the height and a distance of thirty heights on the leeward side [19]. Therefore, to manage and monitor *C. equisetifolia* forests, there is a critical need for an effective tool to accurately detect forest parameters.

Unmanned Aerial Vehicles (UAVs) have become an important technology for assessing forest parameters due to their high spatial resolution, flexibility, and operability [20,21]. Among them, low-cost UAVs with RGB cameras have been widely applied in forest applications due to their ability to detect tree-level parameters accurately (e.g., individual trees and tree height). Notably, the structure from motion (SfM) technique is able to extract three-dimensional (3D) information from UAV imagery [22–24]. Thus, monitoring and detecting the complex 3D structure of forests is feasible using low-cost UAVs with RGB sensors [25–27]. A number of studies have reported the application of UAVs in forest-parameter extraction [28]. For example, Guerra-Hernández et al. [29] reported a relative root mean square error (r$RMSE$) of 4.56% for the extracted tree height of a *Pinus pinea* plantation using high-resolution UAV imagery. Combining the use of a UAV with oblique photogrammetry, Lin et al. [30] assessed the individual tree heights of sparse, subalpine coniferous forest and yielded an accuracy of $RMSE = 1.77$ m. Despite the promising accuracy of forest-parameter assessments achieved in previous studies, UAV flight planning is essential, and the flight parameters should be carefully considered [31–33]. Many researchers have discovered that the flying altitude, image overlap, and other flight-planning settings can impact the quality or useability of final products [33–35]. For example, the resolution of acquired images varies with flying altitude [36,37] and ultimately affects the identification of individual trees [38] and tree crowns [39]. Thus, flight parameters should be carefully considered and aligned with the actual measurement requirements.

An important aspect of processing UAV imagery for forestry applications is to select the appropriate algorithm for individual tree identification and tree height extraction from images [40]. Several algorithms, such as the local maxima algorithm [41], valley following [42], extended-maxima transformation [43], template matching [44], Markov random fields [44], and deep learning [45,46], have been successfully applied in the past decade. Among them, the local maxima algorithm is the most common detection method, primarily based on the maximum value of a moving window of a specified size that is chosen to identify treetops [47,48]. Pouliot et al. [47] stated that the window size is important for detecting individual trees. If the window size is too small, a tree would be divided into several parts. Conversely, the individual trees may not be identified when the window size is too large. For example, Mohan et al. [49] reported an inverse relationship between the fixed tree window size and tree density. Thus, the local maxima algorithm should determine an appropriate window size for object detection [50].

Few studies have considered both the influence of flight parameters and algorithm parameters for detecting individual trees and tree heights. This study explores the influence of flying altitude and the window size of the local maxima algorithm for detecting individual trees and tree heights for *C. equisetifolia* in the Pingtan Comprehensive Pilot Zone. The main purpose of this study is as follows:

(1) To determine the optimal flight altitude for *C. equisetifolia* identification and tree-height estimation;

(2) To assess the optimal extraction parameters of the local maxima algorithm for *C. equisetifolia* identification and tree height estimation.

2. Materials and Methods

2.1. Study Site

This study was conducted in the northeast part of the Pingtan Comprehensive Pilot Zone, Fujian, China (coordinates: 25°37′ N, 119°46′ E) (Figure 1). This region has a marine monsoon climate with an average annual precipitation of 196.2 mm and an average annual temperature of 19.6 °C. The average wind speed reaches 6.9 m/s. The region has serious soil desertification and is often affected by climatic disasters such as typhoons, heavy rain, strong winds, and droughts. *C. equisetifolia* was introduced into the Pingtan Comprehensive Pilot Zone in the 1950s to serve as a windbreak and to stabilize the soil. It was particularly planted in the coastal area with strong winds and poor habitat conditions. Due to poor environmental conditions, *C. equisetifolia* range in size from small bushy shrubs to trees, with small bushy shrubs mainly distributed in the up-wind direction and trees distributed on the leeward side. The study site is covered by *C. equisetifolia* and a few other tree species. Some *C. equisetifolia* were removed and replanted in 2015 due to tree mortality caused by an occurence of disease in 2014.
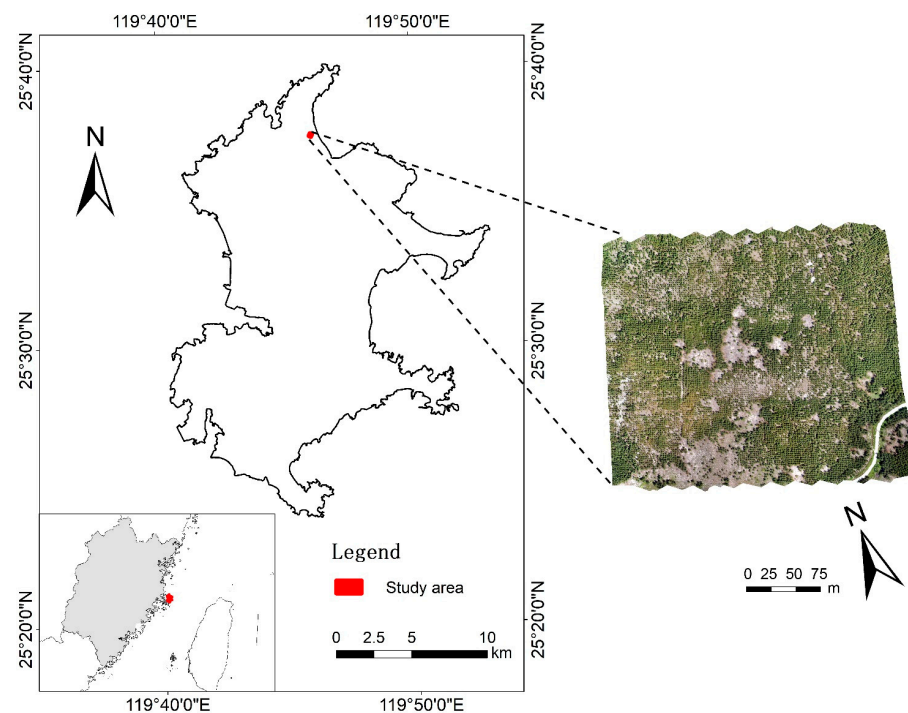

Figure 1. Location of the study site, Pingtan, Fujian, China.

2.2. Field Survey Data

Following UAV imagery collection, field data was collected in September 2021 which included the accurate position of each tree and the corresponding tree height. First, each tree was numbered in the field, and the tree height was measured using a measuring rod. Second, each surveyed tree in the field was marked accurately in the UAV imagery based on GNSS positioning, empty locations in the forest, and other markers to ensure the accurate positions on the image. Finally, a total of 749 *C. equisetifolia* was surveyed in the field, and their corresponding positions on the image were identified (Figure 2). The field-surveyed tree heights varied greatly, ranging from 1.15 to 12.5 m with an average height of 6.54 m.
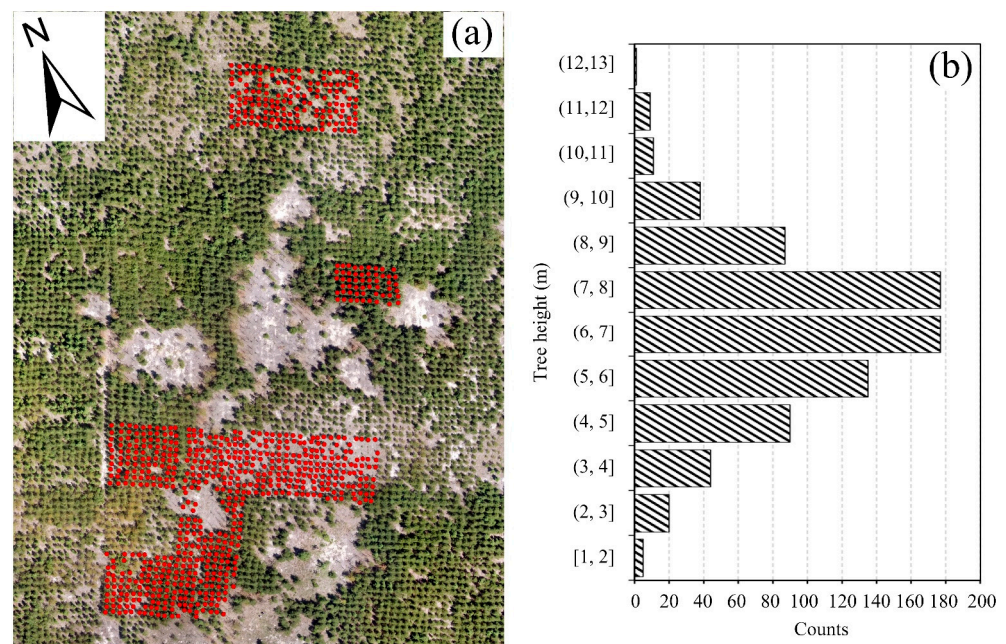
Figure 2. The distribution of field-surveyed trees (**a**) and tree heights (**b**).

2.3. Image Acquisition and Preprocessing

2.3.1. UAV Image Acquisition

UAV imagery was acquired in September 2021 using an integrated camera with six imaging sensors (1600 × 1300 pixels) mounted on a Phantom4-Multispectral(P4M) (https://www.dji.com/p4-multispectral, accessed on 8 September 2021). Six sensors were used: blue (B) (450 ± 16 nm), green (G) (560 ± 16 nm), red (650 ± 16 nm), red edge (RE) (730 ± 16 nm), near-infrared band (NIR) (840 ± 26 nm), and RGB bands. Data was acquired under clear-sky conditions between 10:00 and 14:00 to minimize the influence of tree and cloud shadows. The flight altitude was set at a constant level for each flight to obtain imagery: at 40 m, 60 m, 80 m, 100 m, 120 m, 140 m, 160 m, 180 m, 200 m, 220 m, and 240 m. The flight plan covered approximately 6.5 ha in the study area, with a forward overlap of 85% and a side-lap of 75%. During the flight, the real-time kinematic (RTK) positioning and navigation system was used to ensure high-precision location accuracy, and radiometric calibration was completed using a diffuse plate before each flight.

2.3.2. UAV Image Processing

In this study, DJI Terra software was used to process the UAV imagery (https://www.dji.com/cn/dji-terra, accessed on 28 September 2021). DJI Terra is a UAV aerial survey software which can be used for autonomous route planning, aerial photography, 2D orthophotography, and 3D model reconstruction [51–53]. The built-in SfM algorithm is able to extract 3D information from images with high overlap rates. The output data includes B, G, R, RE, and NIR ortho-mosaics, as well as a digital surface model (DSM).

Next, open ground points were identified manually from non-forest locations. A total of 995 points were used for interpolation in ArcGIS 10.8 (ESRI, Redlands, CA, USA) to create a digital elevation model (DEM). The DEM was generated using the Kriging method. Finally, a canopy height model (CHM) was obtained by subtracting the digital terrain model (DTM) from the DSM. All the processing was repeated to obtain a CHM from flights with different altitudes (Figure 3). Table 1 shows the main parameters for the CHM acquisition process under different flight altitudes.
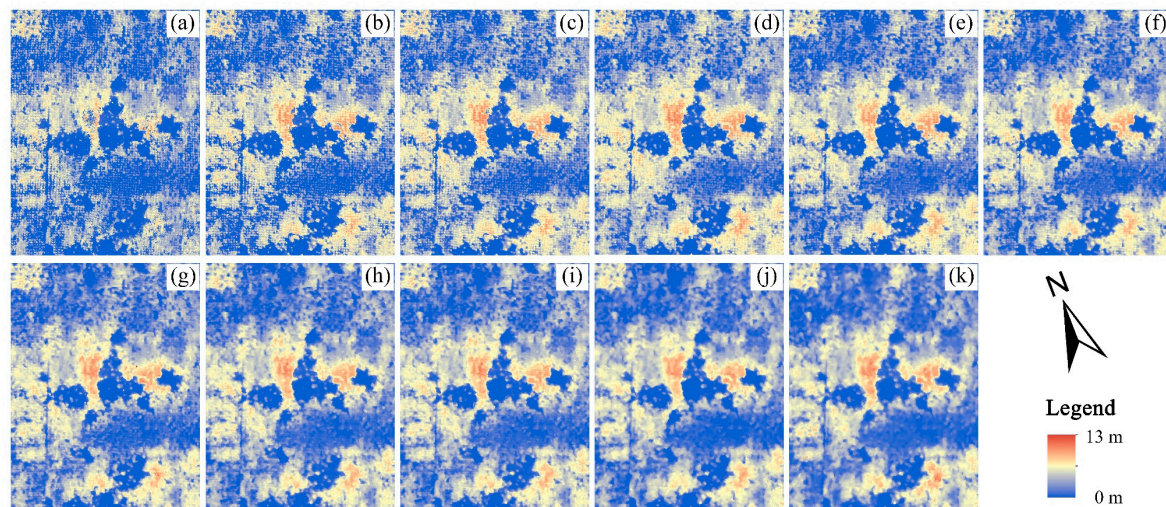
Figure 3. CHMs at different flight altitudes. ((**a**): 40 m; (**b**): 60 m; (**c**): 80 m; (**d**): 100 m; (**e**): 120 m; (**f**): 140 m; (**g**): 160 m; (**h**): 180 m; (**i**): 200 m; (**j**): 220 m; and (**k**): 240 m).

Table 1. UAV image acquisition and pre-processing parameters.

Flight Altitude (Meter)	Flight Time (Minutes)	Number of Acquired Images	SfM Time (Minutes)	CHM Resolution (cm)
40	25.72	4548	14.22	4.9
60	19.21	3252	11.02	7.1
80	14.68	2178	9.11	9.7
100	8.13	1380	5.09	11.8
120	6.23	1038	3.87	14.4
140	6.08	816	2.24	16.7
160	4.68	642	3.47	19.1
180	4.07	546	0.86	21.5
200	3.28	438	0.68	24.0
220	3.53	474	0.77	26.4
240	3.17	426	0.71	28.7

2.4. Individual Tree and Tree Height Extraction

The key feature of the local maxima algorithm is that the CHM's highest values and the brightest pixels in the optical UAV imagery are identified by filtering the image using a moving window [54]. Based on the local maxima algorithm, the highest values in the CHM, representing the treetop were detected in this study [48,49,55,56]. Different window sizes, including the circular smoothing window size (CSWS) and fixed circular window size (FCWS), can impact the accuracy of detecting individual trees and tree heights when using the local maxima algorithm. Thus, an optimal combination of CSWS and FCWS should be determined. To select the optimal CSWS and FCWS for detecting *C. equisetifolia*, the CSWS was set to 0 m (unsmoothed), 0.1 m, 0.2 m, and 0.3 m, while the FCWS was set to 0.4 m, 0.6 m, 0.8 m, 1.0 m, 1.2 m, 1.4 m, 1.6 m, 1.8 m, and 2.0 m separately to determine the optimal combinations.

The main processing was as follows: (1) the CHM was smoothed using the focal statistics tool in ArcGIS 10.8 to reduce the false positive detections (e.g., ground artifacts); (2) the local maximum image with the highest values was identified from the smoothed image using the focal statistics tool; (3) an image with 0 values was generated by subtracting the local maximum image from the smoothed image; (4) values greater than 0.3 m in the image generated in step (3) were filtered as treetops [57]; and (5) the corresponding treetop on the CHM is taken as the value of the tree height [49,56].

2.5. Accuracy Assessment

The recall (*R*), precision (*P*), and *F1* score were used to evaluate the accuracy of individual tree results [58,59]. The equations are as follows:

$$Recall(R) = \frac{TP}{TP + FN} \times 100\% \tag{1}$$

$$Precision(P) = \frac{TP}{TP + FP} \times 100\% \tag{2}$$

$$F1\ score = \frac{2PR}{P + R} \times 100\% \tag{3}$$

where a true positive (*TP*) indicates a correct identification (that is, a tree existed in the ground reference and was correctly identified), a false negative (*FN*) indicates over-identification (that is, a tree existed in the ground reference but was not identified on the image), a false positive (*FP*) indicates under-identification (that is, a tree did not exist in the ground reference but was identified), *R* is the ratio of correctly identified trees to all ground reference trees, *P* is the ratio of correctly identified trees to all detected trees, and the *F1* score represents the overall accuracy, considering omission and commission. A higher *F1* score indicates a better-achieved accuracy for individual tree detection.

The determination coefficient (R^2), *RMSE*, and estimation accuracy (*EA*) were used to evaluate the accuracy of the tree-height results (Equations 4–6) [60–62]. R^2 represents the goodness of fit between tree heights derived from the UAV and the field survey. The *RMSE* is used for error estimation, with a lower value of the *RMSE* indicating a higher accuracy of tree-height results achieved, while a value of *EA* closer to 100% represents a higher accuracy of tree-height results achieved.

$$R^2 = 1 - \frac{\sum_{i=1}^{n} (y_i - x_i)^2}{\sum_{i=1}^{n} (y_i - \overline{x_i})^2} \tag{4}$$

$$RMSE = \sqrt{\frac{1}{n} \sum_{i=1}^{n} (y_i - x_i)^2} \tag{5}$$

$$EA = \left(1 - \frac{RMSE}{\overline{y_i}}\right) \times 100\% \tag{6}$$

where *n* is the number of samples, y_i is the field-surveyed tree height, $\overline{y_i}$ is the mean of the field-surveyed tree height, x_i is the estimated tree height, and $\overline{x_i}$ is the mean of the estimated tree height.

3. Results

3.1. The Effects of Extraction Parameters on Individual Tree Detection (ITD) and Tree-Height Estimation

The results of individual tree detection (ITD) using different extraction parameters based on the local maxima method are presented in Tables 2–4. It is evident that the accuracy of the ITD was impacted by the various combinations of CSWS and FCWS. The values of the *P* and *F1* scores increased and then decreased, and the *R* values decreased with a higher FCWS value under the same CSWS values. The *P* and *F1* score values increased with the higher CSWS values under the same FCWS values. A total of 15 different combinations could meet the requirement for an accurate ITD (*F1* score > 85.00%), including the combination of a 0.1 m–0.3 m CSWS and a 0.4 m–1.0 m FCWS, and the combination of a 0 m CSWS and a 0.6 m–1.0 m FCWS. Particularly when the combinations of CSWS and FCWS were 0.3 m × 0.4 m, 0.2 m × 0.6 m, 0.3 m × 0.6 m, 0.1 m × 0.8 m, 0.2 m × 0.8 m, and 0.3 m × 0.8 m, the value of the *F1* score was higher than 91.00%. The *F1* score decreased significantly when the FCWS was higher than 1.4 m. This can be explained by the *R* value decreasing significantly with the increase in the FCWS.

Table 2. The influence of different combinations of circular smoothing window size (CSWS) and fixed circular window size (FCWS) on the precision (%) of *Casuarina equisetifolia* detection.

CSWS (m)	FCWS (m)								
	0.4	0.6	0.8	1.0	1.2	1.4	1.6	1.8	2.0
0.0	72.67	84.38	91.24	94.24	95.72	95.92	96.10	95.69	94.97
0.1	79.64	87.23	92.88	95.29	96.40	96.72	96.68	96.75	95.91
0.2	86.73	90.48	94.39	96.29	96.97	96.95	96.78	97.25	96.21
0.3	89.72	92.27	95.16	96.61	96.86	97.17	96.93	97.05	96.36

Table 3. The influence of different combinations of CSWS and FCWS on the recall (%) of *C. equisetifolia* detection.

CSWS (m)	FCWS (m)								
	0.4	0.6	0.8	1.0	1.2	1.4	1.6	1.8	2.0
0.0	92.96	91.59	88.07	80.76	71.53	56.99	41.68	33.50	24.18
0.1	93.88	92.73	90.04	83.23	73.40	59.37	43.88	35.33	24.68
0.2	93.19	92.09	89.90	84.23	74.68	59.64	43.97	35.56	24.36
0.3	92.92	92.14	89.76	83.36	74.63	59.73	43.28	34.55	24.18

Table 4. The influence of different combinations of CSWS and FCWS on the *F*1 score (%) of *C. equisetifolia* detection.

CSWS (m)	FCWS (m)								
	0.4	0.6	0.8	1.0	1.2	1.4	1.6	1.8	2.0
0.0	81.57	87.84	89.63	86.98	81.87	71.50	58.14	49.63	38.54
0.1	86.18	89.90	91.44	88.85	83.34	73.58	60.36	51.76	39.26
0.2	89.84	91.28	92.09	89.86	84.38	73.85	60.47	52.07	38.88
0.3	91.29	92.20	92.38	89.50	84.31	73.99	59.84	50.96	38.66

Fifteen different combinations of CSWS and FCWS were used to determine tree heights. The results are presented in Tables 5–7. The accuracy of tree-height estimation declined with an increase in the CSWS when the FCWS was held constant; that is, a higher *RMSE* value and a lower *EA* value were achieved. The accuracy of tree-height estimation increased with an increase in the FCWS when the CSWS was kept constant; that is, higher R^2 and *EA* values and a lower *RMSE* value were achieved. The combination of a 0.1 m CSWS value and a 0.8 m FCWS value was generally determined to be the optimal parameter for ITD and tree-height estimation using the local maxima algorithm.

Table 5. The influence of different combinations of CSWS and FCWS on the tree height extraction for *C. equisetifolia* between UAV-derived image and field measurement (R^2).

CSWS (m)	FCWS (m)			
	0.4	0.6	0.8	1.0
0.0	-	0.87	0.91	0.91
0.1	0.87	0.89	0.89	0.91
0.2	0.88	0.89	0.90	0.91
0.3	0.89	0.89	0.90	0.90

Table 6. The influence of different combinations of CSWS and FCWS on the tree height extraction accuracy (*RMSE*/m) of *C. equisetifolia* detection.

CSWS (m)	FCWS (m)			
	0.4	0.6	0.8	1.0
0.0	-	1.38	1.28	1.26
0.1	1.45	1.39	1.36	1.31
0.2	1.48	1.45	1.41	1.38
0.3	1.48	1.47	1.44	1.42

Table 7. The influence of different combinations of CSWS and FCWS on the tree height extraction accuracy (*EA*/%) of *C. equisetifolia* detection.

CSWS (m)	FCWS (m)			
	0.4	0.6	0.8	1.0
0.0	-	79.07	80.84	81.34
0.1	78.03	78.91	79.49	80.45
0.2	77.65	78.19	78.73	79.47
0.3	77.63	77.81	78.35	78.76

3.2. The Effects of Flight Altitude on ITD

Table 8 shows the accuracy of the ITD using the combination of 0.1 m CSWS and 0.8 m FCWS at different flight altitudes. It is visually apparent that the accuracy of the ITD initially increased and then decreased with the increase in flight altitude. The *P* value was above 85% when the flight altitude was between 60 m and 140 m, and the highest *P* value was achieved at 80 m (P = 94.3%). The *R* value was higher than 85% when the flight altitude was between 40 m and 80 m, and the highest *R* value was achieved when the flight altitude was 60 m (R = 90.04%). The *F*1 score was above 85% when the flight altitude was between 40 m and 80 m, and the highest *F*1 score was achieved when the flight altitude was 60 m (*F*1 score = 91.44%). Therefore, a reasonable accuracy of the ITD was achieved when the flight altitude was between 40 m and 80 m (*F*1 score > 85%).

Table 8. The influence of different UAV flight altitudes on the accuracy of ITD.

Flight Altitude (m)	Precision (%)	Recall (%)	*F*1 Score (%)
40	83.30	89.35	86.22
60	92.88	90.04	91.44
80	94.31	85.60	89.75
100	92.68	75.78	83.38
120	90.18	67.55	77.24
140	88.01	57.36	69.45
160	83.75	49.95	62.58
180	79.46	37.84	51.27
200	74.71	34.96	47.63
220	71.81	29.57	41.89
240	71.59	23.03	34.85

3.3. The Effects of Flight Altitude on Tree Height Estimation

The effects of different flight altitudes on the estimated tree heights are shown in Table 9. The values of the R^2, *RMSE*, and *EA* first increased and then decreased with the increase in flight altitude. The optimal accuracy of tree-height estimation was achieved when the flight altitude was between 60 m and 100 m ($R^2 \geq 0.89$, *RMSE* < 1.60 m, and *EA* > 75%). The R^2 value was higher than 0.85 when the flight altitude was between 60 m and 160 m. Specifically, the highest R^2 value was achieved when the flight altitude was between 80 m and 100 m (R^2 = 0.90). The *RMSE* value was lower than 2.00 m when the

flight altitude was between 40 m and 100 m, and the lowest *RMSE* value was achieved when the flight altitude was 60 m (*RMSE* = 1.36 m). The *EA* value was higher than 75.00% when the flight altitude was between 60 m and 100 m, while the highest *EA* value was achieved when the flight altitude was 60 m (*EA* = 79.49%). However, the accuracy of the tree-height estimation declined rapidly when the flight altitude was higher than 100 m.

Table 9. The influence of different UAV flight altitudes on the tree-height estimation for *C. equisetifolia* between UAV-derived images and field measurements.

Flight Altitude (m)	R^2	RMSE/m	EA/%
40	0.81	1.69	74.39
60	0.89	1.36	79.49
80	0.90	1.59	76.28
100	0.90	1.59	76.38
120	0.87	2.21	67.88
140	0.88	2.49	65.83
160	0.86	2.74	60.43
180	0.82	2.83	60.16
200	0.79	2.98	59.21
220	0.81	3.12	57.28
240	0.72	3.03	59.72

In summary, the highest accuracy of the ITD and tree-height estimation was achieved at a flight height of 60 m. However, it is recommended to use a flight height of 80 m for *C. equisetifolia* identification and tree-height detection, mainly because of the shorter flight time, SfM time, and fewer images to process when compared to a flight height of 60 m (Table 1). Therefore, a flight height of 80 m was selected as the UAV parameter in this study, which yielded an *F*1 score = 81.75% for ITD and an *EA* = 76.28% for tree-height estimation (Figure 4). The results of *C. equisetifolia* identification and tree-height detection are shown in Figure 5.
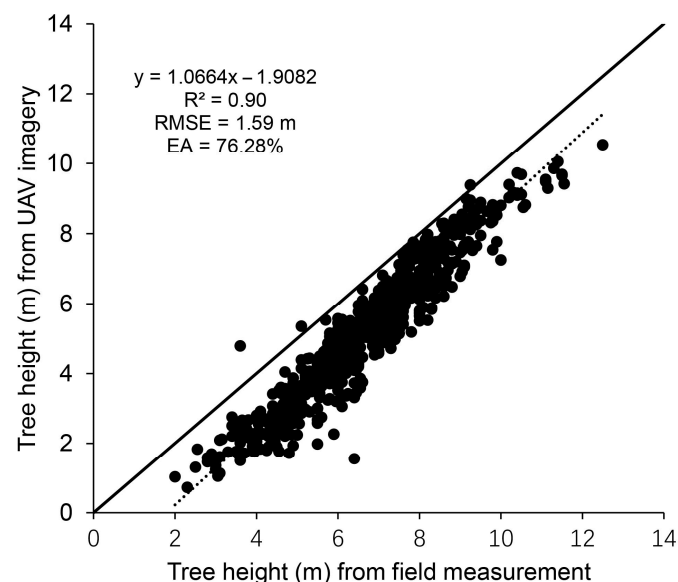

Figure 4. Linear regression of tree height between the field measurements and UAV imagery estimation at a flight height of 80 m.
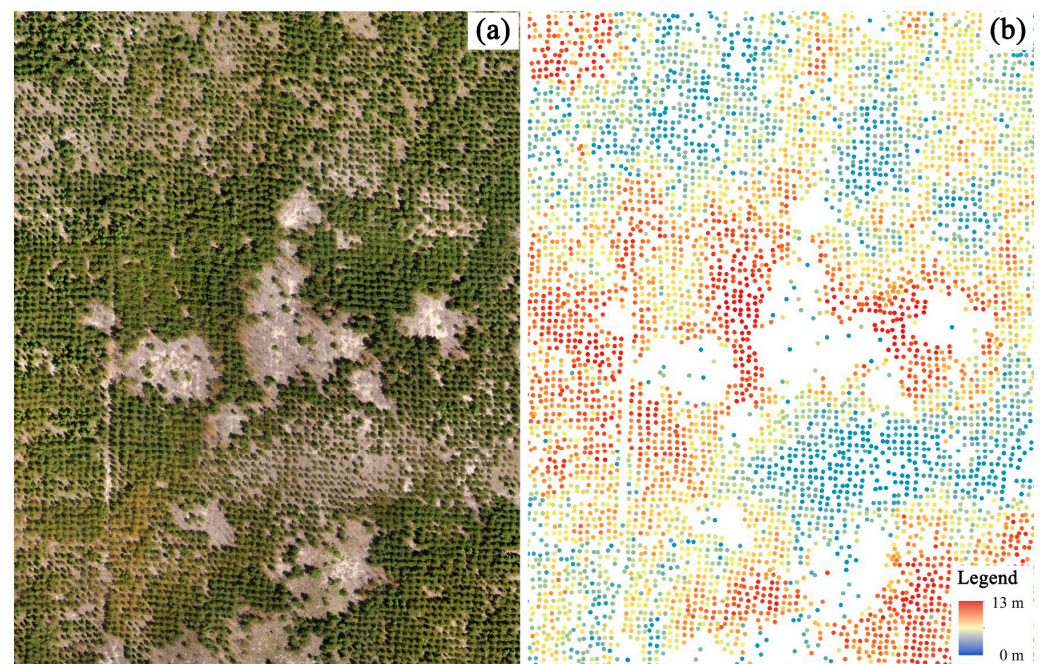
Figure 5. The results of *Casuarina equisetifolia* identification and tree-height detection at the flight height of 80 m. (**a**) UAV image and (**b**) results of ITD and tree-height detection.

4. Discussion

This study focused on determining the optimal flight altitude and parameters of the local maxima algorithm to improve the accuracy of *C. equisetifolia* identification and tree-height estimation results. Although previous studies have mentioned the ability of *C. equisetifolia* to provide a windbreak, few studies reported monitoring this tree species effectively in the coastal regions. Our results showed the optimal accuracy of ITD and tree-height estimation when the flight altitude was 60 m and the combination of the CSWS and FCWS was 0.1 m × 0.8 m for the local maxima algorithm. This study can help acquire accurate forest-characterization information from UAVs at the tree-level, which contributes to forest management and forest tree identification.

Flight altitude is an important variable affecting UAV image resolution, ultimately affecting the accuracy of ITD and tree-height estimation [36,37,63]. Our study found that the image quality could meet the accuracy requirement of ITD and tree-height estimation when the flight altitude was between 60 m and 80 m. Similar results have been reported in previous studies. For example, Dandois et al. [36,37,63] stated that a flight altitude of 80 m is optimal for mapping forest structure, considering image collection and processing efficiency. Comparing three altitudes above ground level (65 m, 90 m, and 115 m) for UAV image collection, Swayze et al. [64] reported that 65 m was the optimal flight altitude for detecting forest parameters (e.g., tree height, DBH, and density).

Image overlap influences the forest-parameter estimation less than flight altitude. There is a consensus that >75% forward overlap and 60%–80% side-lap are recommended for UAV image acquisition [35]. Similarly, Tu et al. [33] demonstrated that when the forward overlap was less than 80% the accuracy of the tree-height estimation decreased significantly, and that the optimal side-lap was between 70% and 80%. In this context, the forward overlap and side-lap in this study were set at 85% and 75%, respectively.

Previous studies have reported that a higher accuracy of forest-parameter estimation results when a lower flight altitude was used [37]. However, our study indicated that a flight altitude of 40 m is not optimal for detecting *C. equisetifolia* at the individual-tree level. This may be explained by declining image overlap in higher tree-height areas, which could decrease the accuracy of a 3D-generated reconstruction by SfM (Figure 6). Contrarily, it has few impacts on the areas of lower tree height. Therefore, the appropriate

flight height of a UAV should be determined for monitoring different tree species. For instance, Johansen et al. [37] suggested that a flight height of 30 m was the optimal UAV parameter for tree crown perimeter, area, and height estimation compared to flight heights of 50 m and 70 m. This can be explained by the surveyed tree heights in the study by Johansen et al., which were mainly between 2 m and 3 m and would be subject to few impacts on image overlap.
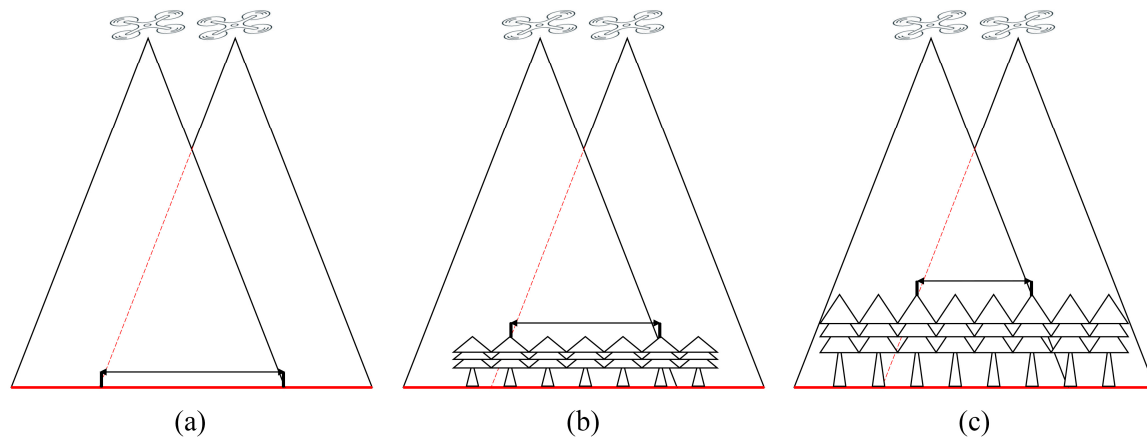

Figure 6. Example of the influence of tree height on the overlaps for UAV images in a (**a**) non-forest area; (**b**) forest with low tree height; and (**c**) forest with high tree height.

The UAV flight altitude of 80 m in this study had clear advantages over a 60 m flight altitude. One advantage is that one single flight was able to cover the study area of approximately 6.5 ha using the charge of a single battery at the height of 80 m, while two batteries are needed to complete the flight at the height of 60 m. Moreover, a longer flight time with battery replacement would increase the risk of shadows from cloud cover. In addition, the number of obtained UAV images at a height of 80 m (3252) is less than the number of images acquired at 60 m (2178). Having fewer images can also reduce image-processing time. The SfM times were 11.02 and 9.11 minutes under the heights of 60 m and 80 m, respectively. Torres-Sanchez et al. [65] compared imagery collected at 50 m and 100 m above ground level for mapping the structural parameters of olive trees and reported that both the time of flight as well as the multi-spectral images and RGB image processing were reduced from 47 min to 13 min and from 5 h 15 min to 1 h 8 min, respectively. Therefore, considering the efficiency of UAV image acquisition and processing, as well as the accuracy of ITD and tree-height detection, a flight altitude of 80 m was selected for ITD and tree-height estimation.

The local maxima algorithm is the most commonly used classical method, and window size is a critical factor affecting the accuracy of the ITD and tree-height estimation [50]. Our study determined the optimal combination of a 0.1 m CSWS and a 0.8 m FCWS for ITD and tree-height estimation. From Tables 4 and 7, it can be seen that when the FCWS was 0.8 m, the accuracy of the ITD increased with an increase in the CSWS. In contrast, the accuracy of tree-height estimation decreased with an increase in the CSWS. This is because the smoothed image becomes smoother with an increase in CSWS and outliers have less influence on the ITD, while the UAV generally underestimated the tree height (Figure 4) for *C. equisetifolia* and the accuracy of the tree-height estimation would be lower if a larger CSWS was used. Thus, a CSWS of 0.1 m was adopted in this study to balance the accuracy of the ITD and tree-height estimation.

In this study, the UAV-derived tree heights were underestimated at all flight altitudes. Previous studies have reported two reasons to explain the tree-height underestimation. One possible explanation is that the DTM is overestimated, which serves to cover the base of trunk information. This mainly occurs in areas with high forest coverage or abundant understory vegetation where it is challenging to obtain the ground position accurately [57,66,67].

Another reason is that the resolution of the CHM is relative coarse compared to the size of treetops, which can result in the loss of treetops in the CHM [57,62,67]. In our study, it was possible to obtain the ground position accurately because of the evenly distributed trees. Therefore, the underestimated tree heights in our study are most likely explained by the coarse resolution of CHM, which resulted in the loss of treetops. In this study, the resolution of CHM was 9.7 cm when the flight altitude was 80 m. The coarse resolution of the CHM relative to the thin treetop results in the underestimation of tree heights. The tree heights of Figure 7a,b were 4.7 m and 5.1 m in the field measurement, respectively. The estimated tree heights from the UAV image were 2.98 m and 2.92 m at the altitude of 80 m, respectively, and the tree heights were underestimated by 1.72 m and 2.18 m. As can be seen from Figure 7, the tree in Figure 7b was more seriously underestimated than the tree in Figure 7a due to the slender and obvious treetop.
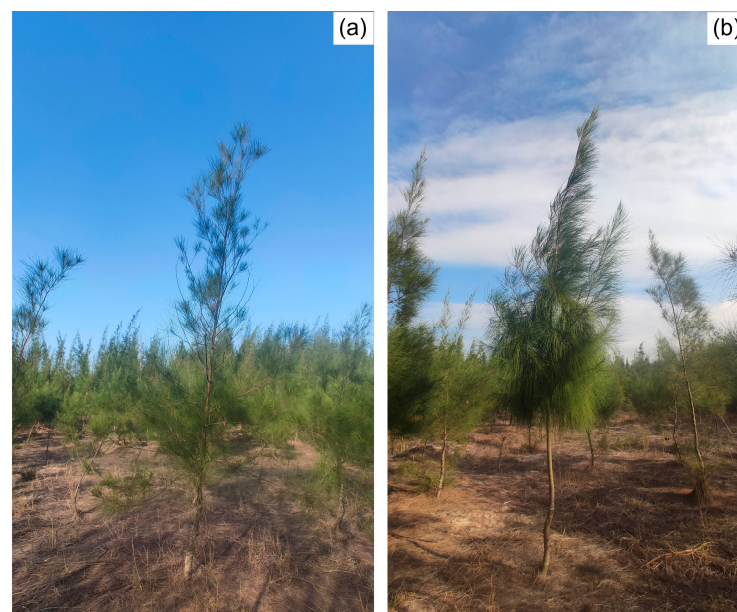
Figure 7. *C. equisetifolia* with different crown shapes (**a**,**b**) in the field.

The study site is located in a sensitive island environment, which results in the treetops of *C. equisetifolia* being exposed to heavy wind erosion. The top of a tall *C. equisetifolia* is more likely become full than the shorter trees under heavy wind erosion. Therefore, the identification of shorter trees is more often underestimated in the study area. Similar studies have reported that UAV-derived tree height was underestimated, but this deviation can be modified if it is consistent [67,68].

Casuarina equisetifolia was widely introduced into the coastal areas of Guangdong and Fujian, China, because of its ability to stabilize sandy soils [4,5], drought and salt resistance [6,7], soil-quality improvement potential, and soil-rehabilitation ability [2,8]. However, some *C. equisetifolia* is susceptible to plant diseases and insect pests due to being planted in a pure stand. Therefore, detecting individual trees is helpful for monitoring the status of *C. equisetifolia* forest stands. In addition, monitoring can identify open forest gaps and provide information on dead trees, such as their number and position, to support forest management (Figure 5).

In addition to individual tree identification and tree-height estimation, other forest parameters can be estimated using UAV-derived DSMs and multi-spectral imagery, including tree crowns [29,56], DBH [64,69,70], and biomass [71,72]. More detailed information can be detected rapidly and accurately using UAVs in the future as the capabilities of UAVs increase over time. Additionally, UAVs can track long-term dynamic changes in forest parameters using flights over time [73–76]. Low-cost consumer UAVs have been widely used in forestry applications because of their affordable characteristics. In this study,

the proposed workflow was designed for the Phantom4-Multispectral UAV, so the flight parameters may not be directly suitable for other sensors. Nevertheless, the proposed procedure for evaluating the optimal flight altitude and extraction parameters will inform other workflows.

5. Conclusions

Detecting individual trees and tree heights is critical information for managing *C. equisetifolia*, considering its characteristics of sandy-soil stabilization and windbreak ability in coastal regions. This study assessed the accuracy of individual tree and tree-height results based on the collected UAV imagery from different flight altitudes and the local maxima algorithm to determine the appropriate, optimal flight altitude and extraction parameters for detecting individual trees and tree heights. The results demonstrated that the flight altitude should not be minimized for optimal results. When the flight altitude was 60 m and the combination of the CSWS and FCWS was 0.1 m and 0.8 m, respectively, of the local maxima algorithm, the highest accuracies of ITD and tree-height estimation were achieved (*F*1 score = 91.44% for ITD and *EA* = 79.49% for tree height estimation). Excellent accuracy was achieved when the flight altitude ranged from 60 m to 80 m (*F*1 score > 85.00% for ITD, *EA* > 75.00% for tree-height estimation). It is suggested that a flight altitude of 80 m is suitable for detecting *C. equisetifolia* because a UAV can cover a larger area using a single battery charge. This study assists forest practitioners in management and provides accurate information on using UAVs in forestry.

References

1. Pinyopusarerk, K.; Williams, E.R. Range-wide provenance variation in growth and morphological characteristics of *Casuarina equisetifolia* grown in Northern Australia. *For. Ecol. Manag.* **2000**, *134*, 219–232. [CrossRef]
2. Diagne, N.; Diouf, D.; Svistoonoff, S.; Kane, A.; Noba, K.; Franche, C.; Bogusz, D.; Duponnois, R. Casuarina in Africa: Distribution, role and importance of arbuscular mycorrhizal, ectomycorrhizal fungi and Frankia on plant development. *J. Environ. Manag.* **2013**, *128*, 204–209. [CrossRef] [PubMed]
3. Parrotta, J.A.; Baker, D.D.; Fried, M. Application of 15 N-enrichment methodologies to estimate nitrogen fixation in *Casuarina equisetifolia*. *Can. J. For. Res.* **1994**, *24*, 201–207. [CrossRef]
4. Ndiaye, P.; Mailly, D.; Pineau, M.; Margolis, H.A. Growth and yield of *Casuarina equisetifolia* plantations on the coastal sand dunes of Senegal as a function of microtopography. *For. Ecol. Manag.* **1993**, *56*, 13–28. [CrossRef]
5. Zhong, C.; Zhang, Y.; Chen, Y.; Jiang, Q.; Chen, Z.; Liang, J.; Pinyopusarerk, K.; Franche, C.; Bogusz, D. Casuarina research and applications in China. *Symbiosis* **2010**, *50*, 107–114. [CrossRef]
6. El-Lakany, M.H. A review of breeding drought resistant Casuarina for shelterbelt establishment in arid regions with special reference to Egypt. *For. Ecol. Manag.* **1983**, *6*, 129–137. [CrossRef]
7. Tani, C.; Sasakawa, H. Salt tolerance of *Casuarina equisetifolia* and Frankia Ceq1 strain isolated from the root nodules of C. equisetifolia. *Soil Sci. Plant Nutr.* **2003**, *49*, 215–222. [CrossRef]
8. Karthikeyan, A.; Deeparaj, B.; Nepolean, P. Reforestation in bauxite mine spoils with *Casuarina equisetifolia* frost. And beneficial microbes. *For. Trees Livelihoods* **2009**, *19*, 153–165. [CrossRef]

9. Meng, J.; Bai, Y.; Zeng, W.; Ma, W. A management tool for reducing the potential risk of windthrow for coastal *Casuarina equisetifolia* L. stands on Hainan Island, China. *Eur. J. For. Res.* **2017**, *136*, 543–554. [CrossRef]

10. Samarakoon, M.B.; Tanaka, N.; Iimura, K. Improvement of effectiveness of existing *Casuarina equisetifolia* forests in mitigating tsunami damage. *J. Environ. Manag.* **2013**, *114*, 105–114. [CrossRef]

11. Jeong, S.; Lee, S. Effects of windbreak Forest according to tree species and planting methods based on wind tunnel experiments. *For. Sci. Technol.* **2020**, *16*, 188–194. [CrossRef]

12. Lee, J.; Yen, L.; Lee, M. Wind affects the growth, root anchorage and tensile strength of Australian pine (*Casuarina equisetifolia*) seedlings. *J. For. Res.* **2019**, *24*, 219–229. [CrossRef]

13. Chopping, M.; Moisen, G.G.; Su, L.; Laliberte, A.; Rango, A.; Martonchik, J.V.; Peters, D.P.C. Large area mapping of southwestern forest crown cover, canopy height, and biomass using the NASA Multiangle Imaging Spectro-Radiometer. *Remote Sens. Environ.* **2008**, *112*, 2051–2063. [CrossRef]

14. Bitog, J.P.; Lee, I.B.; Hwang, H.S.; Shin, M.H.; Hong, S.W.; Seo, I.H.; Mostafa, E.; Pang, Z. A wind tunnel study on aerodynamic porosity and windbreak drag. *For. Sci. Technol.* **2011**, *7*, 8–16. [CrossRef]

15. Ba Thuy, N.; Tanimoto, K.; Tanaka, N.; Harada, K.; Iimura, K. Effect of open gap in coastal forest on tsunami run-up—Investigations by experiment and numerical simulation. *Ocean Eng.* **2009**, *36*, 1258–1269. [CrossRef]

16. Tanaka, N.; Nandasena, N.A.K.; Jinadasa, K.B.S.N.; Sasaki, Y.; Tanimoto, K.; Mowjood, M.I.M. Developing effective vegetation bioshield for tsunami protection. *Civ. Eng. Environ. Syst.* **2009**, *26*, 163–180. [CrossRef]

17. Heisler, G.M.; Dewalle, D.R. Effects of windbreak structure on wind flow. *Agric. Ecosyst. Environ.* **1988**, *22–23*, 41–69. [CrossRef]

18. Zhang, K.; Qu, J.; Zhang, X.; Zhao, L.; Li, S. Protective efficiency of railway arbor-shrub windbreak forest belts in Gobi regions: Numerical simulation and wind tunnel tests. *Front. Environ. Sci.* **2022**, *10*, 513. [CrossRef]

19. Brandle, J.R.; Hodges, L.; Zhou, X.H. Windbreaks in North American agricultural systems. *Agrofor. Syst.* **2004**, *61–62*, 65–78.

20. Shakhatreh, H.; Sawalmeh, A.H.; Al-Fuqaha, A.; Dou, Z.; Almaita, E.; Khalil, I.; Othman, N.S.; Khreishah, A.; Guizani, M. Unmanned Aerial Vehicles (UAVs): A Survey on civil applications and key research challenges. *Ieee Access* **2019**, *7*, 48572–48634. [CrossRef]

21. Torresan, C.; Berton, A.; Carotenuto, F.; Di Gennaro, S.F.; Gioli, B.; Matese, A.; Miglietta, F.; Vagnoli, C.; Zaldei, A.; Wallace, L. Forestry applications of UAVs in Europe: A review. *Int. J. Remote Sens.* **2017**, *38*, 2427–2447. [CrossRef]

22. James, M.R.; Robson, S. Straightforward reconstruction of 3D surfaces and topography with a camera: Accuracy and geoscience application. *J. Geophys. Res. Earth Surf.* **2012**, *117*, F3. [CrossRef]

23. Puliti, S.; Ørka, H.; Gobakken, T.; Næsset, E. Inventory of small forest areas using an unmanned aerial system. *Remote Sens.* **2015**, *7*, 9632–9654. [CrossRef]

24. Ullman, S. The interpretation of structure from motion. *Proc. R. Soc. Lond. Ser. B. Biol. Sci.* **1979**, *203*, 405–426.

25. Bohlin, J.; Wallerman, J.; Fransson, S.J.E. Deciduous forest mapping using change detection of multi-temporal canopy height models from aerial images acquired at leaf-on and leaf-off conditions. *Scand. J. Forest Res.* **2016**, *31*, 517–525. [CrossRef]

26. Chen, S.; Liang, D.; Ying, B.; Zhu, W.; Zhou, G.; Wang, Y. Assessment of an improved individual tree detection method based on local-maximum algorithm from unmanned aerial vehicle RGB imagery in overlapping canopy mountain forests. *Int. J. Remote Sens.* **2021**, *42*, 106–125. [CrossRef]

27. Guerra-Hernández, J.; Cosenza, D.N.; Rodriguez, L.C.E.; Silva, M.; Tomé, M.; Díaz-Varela, R.A.; González-Ferreiro, E. Comparison of ALS- and UAV(SfM)-derived high- density point clouds for individual tree detection in Eucalyptus plantations. *Int. J. Remote Sens.* **2018**, *15–16*, 5211–5235. [CrossRef]

28. Kansanen, K.; Vauhkonen, J.; Lähivaara, T.; Seppänen, A.; Maltamo, M.; Mehtätalo, L. Estimating forest stand density and structure using Bayesian individual tree detection, stochastic geometry, and distribution matching. *Isprs-J. Photogramm. Remote Sens.* **2019**, *152*, 66–78. [CrossRef]

29. Guerra-Hernández, J.; Gonzalez-Ferreiro, E.; Sarmento, A.; Silva, J.; Nunes, A.; Correia, A.C.; Fontes, L.; Tomé, M.; Diaz-Varela, R. Using high resolution UAV imagery to estimate tree variables in Pinus pinea plantation in Portugal. *For. Syst.* **2016**, *25*, 16. [CrossRef]

30. Lin, J.; Wang, M.; Ma, M.; Lin, Y. Aboveground tree biomass estimation of sparse subalpine coniferous forest with UAV oblique photography. *Remote Sens.* **2018**, *10*, 1849. [CrossRef]

31. Aasen, H.; Honkavaara, E.; Lucieer, A.; Zarco-Tejada, P. Quantitative remote sensing at ultra-high resolution with UAV Spectroscopy: A review of sensor technology, measurement procedures, and data correction workflows. *Remote Sens.* **2018**, *10*, 1091. [CrossRef]

32. Roth, L.; Hund, A.; Aasen, H. PhenoFly planning tool: Flight planning for high-resolution optical remote sensing with unmanned areal systems. *Plant Methods* **2018**, *14*, 116. [CrossRef]

33. Tu, Y.; Phinn, S.; Johansen, K.; Robson, A.; Wu, D. Optimising drone flight planning for measuring horticultural tree crop structure. *Isprs-J. Photogramm. Remote Sens.* **2020**, *160*, 83–96. [CrossRef]

34. Dandois, J.; Olano, M.; Ellis, E. Optimal altitude, overlap, and weather conditions for computer vision UAV estimates of forest structure. *Remote Sens.* **2015**, *7*, 13895–13920. [CrossRef]

35. Singh, K.K.; Frazier, A.E. A meta-analysis and review of unmanned aircraft system (UAS) imagery for terrestrial applications. *Int. J. Remote Sens.* **2018**, *39*, 5078–5098. [CrossRef]

36. Frey, J.; Kovach, K.; Stemmler, S.; Koch, B. UAV Photogrammetry of forests as a vulnerable process. A sensitivity analysis for a structure from motion RGB-image pipeline. *Remote Sens.* **2018**, *10*, 912. [CrossRef]

37. Johansen, K.; Raharjo, T.; McCabe, M. Using multi-spectral UAV imagery to extract tree crop structural properties and assess pruning effects. *Remote Sens.* **2018**, *10*, 854. [CrossRef]

38. Zarco-Tejada, P.J.; Diaz-Varela, R.; Angileri, V.; Loudjani, P. Tree height quantification using very high resolution imagery acquired from an unmanned aerial vehicle (UAV) and automatic 3D photo-reconstruction methods. *Eur. J. Agron.* **2014**, *55*, 89–99. [CrossRef]

39. Yin, D.; Wang, L. Individual mangrove tree measurement using UAV-based LiDAR data: Possibilities and challenges. *Remote Sens. Environ.* **2019**, *223*, 34–49. [CrossRef]

40. Dalponte, M.; Ørka, H.O.; Ene, L.T.; Gobakken, T.; Næsset, E. Tree crown delineation and tree species classification in boreal forests using hyperspectral and ALS data. *Remote Sens. Environ.* **2014**, *140*, 306–317. [CrossRef]

41. Silva, C.A.; Hudak, A.T.; Vierling, L.A.; Loudermilk, E.L.; O'Brien, J.J.; Hiers, J.K.; Jack, S.B.; Gonzalez-Benecke, C.; Lee, H.; Falkowski, M.J.; et al. Imputation of individual longleaf pine (Pinus palustris Mill.) tree attributes from field and lidar data. *Can. J. Remote Sens.* **2016**, *42*, 554–573. [CrossRef]

42. Gougeon, F.A. A crown-following approach to the automatic delineation of individual tree crowns in high spatial resolution aerial images. *Can. J. Remote Sens.* **1995**, *21*, 274–284. [CrossRef]

43. Lee, J.; Biging, G.S.; Fisher, J.B. An individual tree-based automated registration of aerial images to lidar data in a forested area. *Photogramm. Eng. Remote Sens.* **2016**, *82*, 699–710. [CrossRef]

44. Larsen, M.; Eriksson, M.; Descombes, X.; Perrin, G.; Brandtberg, T.; Gougeon, F.A. Comparison of six individual tree crown detection algorithms evaluated under varying forest conditions. *Int. J. Remote Sens.* **2011**, *32*, 5827–5852. [CrossRef]

45. Kattenborn, T.; Leitloff, J.; Schiefer, F.; Hinz, S. Review on Convolutional Neural Networks (CNN) in vegetation remote sensing. *Isprs-J. Photogramm. Remote Sens.* **2021**, *173*, 24–49. [CrossRef]

46. Hao, Z.; Post, C.J.; Mikhailova, E.A.; Lin, L.; Liu, J.; Yu, K. How does sample labeling and distribution affect the accuracy and efficiency of a deep learning model for individual tree-crown detection and delineation. *Remote Sens.* **2022**, *14*, 1561. [CrossRef]

47. Pouliot, D.A.; King, D.J.; Bell, F.W.; Pitt, D.G. Automated tree crown detection and delineation in high-resolution digital camera imagery of coniferous forest regeneration. *Remote Sens. Environ.* **2002**, *82*, 322–334. [CrossRef]

48. Wulder, M.; Niemann, K.O.; Goodenough, D.G. Error reduction methods for local maximum filtering of high spatial resolution imagery for locating trees. *Can. J. Remote Sens.* **2002**, *28*, 621–628. [CrossRef]

49. Mohan, M.; Silva, C.; Klauberg, C.; Jat, P.; Catts, G.; Cardil, A.; Hudak, A.; Dia, M. Individual tree detection from unmanned aerial vehicle (UAV) derived canopy height model in an open canopy mixed conifer forest. *Forests* **2017**, *8*, 340. [CrossRef]

50. Mohan, M.; Mendonça, B.A.F.D.; Silva, C.A.; Klauberg, C.; de Saboya Ribeiro, A.S.; Araújo, E.J.G.D.; Monte, M.A.; Cardil, A. Optimizing individual tree detection accuracy and measuring forest uniformity in coconut (*Cocos nucifera* L.) plantations using airborne laser scanning. *Ecol. Model.* **2019**, *409*, 108736. [CrossRef]

51. Gallardo-Salazar, J.L.; Pompa-García, M. Detecting individual tree attributes and multispectral indices using Unmanned Aerial Vehicles: Applications in a pine clonal orchard. *Remote Sens.* **2020**, *12*, 4144. [CrossRef]

52. Lu, H.; Fan, T.; Ghimire, P.; Deng, L. Experimental evaluation and consistency comparison of UAV multispectral minisesors. *Remote Sens.* **2020**, *12*, 2542. [CrossRef]

53. Syetiawan, A.; Gularso, H.; Kusnadi, G.I.; Pramudita, G.N. Precise topographic mapping using direct georeferencing in UAV. *IOP Conf. Ser. Earth Environ. Sci.* **2020**, *500*, 12029. [CrossRef]

54. Xu, X.; Zhou, Z.; Tang, Y.; Qu, Y. Individual tree crown detection from high spatial resolution imagery using a revised local maximum filtering. *Remote Sens. Environ.* **2021**, *258*, 112397. [CrossRef]

55. Hao, Z.; Lin, L.; Post, C.J.; Jiang, Y.; Li, M.; Wei, N.; Yu, K.; Liu, J. Assessing tree height and density of a young forest using a consumer unmanned aerial vehicle (UAV). *New For.* **2021**, *52*, 843–862. [CrossRef]

56. Panagiotidis, D.; Abdollahnejad, A.; Surový, P.; Chiteculo, V. Determining tree height and crown diameter from high-resolution UAV imagery. *Int. J. Remote Sens.* **2017**, *38*, 2392–2410. [CrossRef]

57. Tu, Y.; Johansen, K.; Phinn, S.; Robson, A. Measuring canopy structure and condition using multi-spectral UAS imagery in a horticultural environment. *Remote Sens.* **2019**, *11*, 269. [CrossRef]

58. Goutte, C.; Gaussier, E. A probabilistic interpretation of precision, recall and F-score, with implication for evaluation. In Proceedings of the 27th European Conference on IR Research, Santiago de Compostela, Spain, 21–23 March 2005; Volume 3408, pp. 345–359.

59. Sokolova, M.; Japkowicz, N.; Szpakowicz, S. Beyond accuracy, F-score and ROC: A family of discriminant measures for performance evaluation. In Proceedings of the 19th Australian Joint Conference on Artificial Intelligence, Hobart, Australia, 4–8 December 2006; Springer: Berlin/Heidelberg, Germany; Volume 4304, pp. 1015–1021.

60. Hyndman, R.J.; Koehler, A.B. Another look at measures of forecast accuracy. *Int. J. Forecast.* **2006**, *22*, 679–688. [CrossRef]

61. Persson, H.; Perko, R. Assessment of boreal forest height from WorldView-2 satellite stereo images. *Remote Sens. Lett.* **2016**, *7*, 1150–1159. [CrossRef]

62. Wu, D.; Johansen, K.; Phinn, S.; Robson, A.; Tu, Y. Inter-comparison of remote sensing platforms for height estimation of mango and avocado tree crowns. *Int. J. Appl. Earth Obs. Geoinf.* **2020**, *89*, 102091. [CrossRef]

63. Seifert, E.; Seifert, S.; Vogt, H.; Drew, D.; van Aardt, J.; Kunneke, A.; Seifert, T. Influence of drone altitude, image overlap, and optical sensor resolution on multi-view reconstruction of forest images. *Remote Sens.* **2019**, *11*, 1252. [CrossRef]

64. Swayze, N.C.; Tinkham, W.T.; Vogeler, J.C.; Hudak, A.T. Influence of flight parameters on UAS-based monitoring of tree height, diameter, and density. *Remote Sens. Environ.* **2021**, *263*, 112540. [CrossRef]

65. Torres-Sánchez, J.; López-Granados, F.; Serrano, N.; Arquero, O.; Peña, J.M. High-throughput 3-D monitoring of agricultural-tree plantations with Unmanned Aerial Vehicle (UAV) technology. *PLoS One* **2015**, *10*, e130479. [CrossRef]

66. Fawcett, D.; Azlan, B.; Hill, T.C.; Kho, L.K.; Bennie, J.; Anderson, K. Unmanned aerial vehicle (UAV) derived structure-from-motion photogrammetry point clouds for oil palm (Elaeis guineensis) canopy segmentation and height estimation. *Int. J. Remote Sens.* **2019**, *40*, 7538–7560. [CrossRef]

67. Swinfield, T.; Lindsell, J.A.; Williams, J.V.; Harrison, R.D.; Agustiono; Habibi; Gemita, E.; Schönlieb, C.B.; Coomes, D.A. Accurate measurement of tropical forest canopy heights and aboveground carbon using structure from motion. *Remote Sens.* **2019**, *11*, 928. [CrossRef]

68. Jensen, J.; Mathews, A. Assessment of image-based point cloud products to generate a bare earth surface and estimate canopy heights in a woodland ecosystem. *Remote Sens.* **2016**, *8*, 50. [CrossRef]

69. Carr, J.C.; Slyder, J.B. Individual tree segmentation from a leaf-off photogrammetric point cloud. *Int. J. Remote Sens.* **2018**, *39*, 5195–5210. [CrossRef]

70. Iizuka, K.; Yonehara, T.; Itoh, M.; Kosugi, Y. Estimating tree height and diameter at breast height (dbh) from digital surface models and orthophotos obtained with an Unmanned Aerial System for a Japanese Cypress (*Chamaecyparis obtusa*) Forest. *Remote Sens.* **2018**, *10*, 13. [CrossRef]

71. Jaakkola, A.; Hyyppä, J.; Yu, X.; Kukko, A.; Kaartinen, H.; Liang, X.; Hyyppä, H.; Wang, Y. Autonomous collection of forest field reference-the outlook and a first step with UAV laser scanning. *Remote Sens.* **2017**, *9*, 785. [CrossRef]

72. Otero, V.; Van De Kerchove, R.; Satyanarayana, B.; Martínez-Espinosa, C.; Fisol, M.A.B.; Ibrahim, M.R.B.; Sulong, I.; Mohd-Lokman, H.; Lucas, R.; Dahdouh-Guebas, F. Managing mangrove forests from the sky: Forest inventory using field data and Unmanned Aerial Vehicle (UAV) imagery in the Matang Mangrove Forest Reserve, peninsular Malaysia. *For. Ecol. Manag.* **2018**, *411*, 35–45. [CrossRef]

73. Crosby, M.K.; Matney, T.G.; Schultz, E.B.; Evans, D.L.; Grebner, D.L.; Londo, H.A.; Rodgers, J.C.; Collins, C.A. Consequences of Landsat Image Strata Classification Errors on Bias and Variance of Inventory Estimates: A forest inventory case study. *IEEE J. Sel. Top. Appl. Earth Observ. Remote Sens.* **2017**, *10*, 243–251. [CrossRef]

74. Ding, Z.; Li, R.; O'Connor, P.; Zheng, H.; Huang, B.; Kong, L.; Xiao, Y.; Xu, W.; Ouyang, Z. An improved quality assessment framework to better inform large-scale forest restoration management. *Ecol. Indic.* **2021**, *123*, 107370. [CrossRef]

75. Galidaki, G.; Zianis, D.; Gitas, I.; Radoglou, K.; Karathanassi, V.; Tsakiri-Strati, M.; Woodhouse, I.; Mallinis, G. Vegetation biomass estimation with remote sensing: Focus on forest and other wooded land over the Mediterranean ecosystem. *Int. J. Remote Sens.* **2017**, *38*, 1940–1966. [CrossRef]

76. Gu, L.; Gong, Z.; Bu, Y. Forest quality dynamic change and its driving factors accompanied by forest transition in China. *Forests* **2021**, *12*, 733. [CrossRef]